



Experimental Study of Dissolution-Alteration of Amphibole in a Hydrothermal Environment

LI Yongli¹, HUANG Fei^{1,2,*}, GAO Wenyuan¹, TANG Xu³, REN Yaqun¹, MENG Lin¹ and ZHANG Zhibin¹

¹ Key Laboratory of Ministry of Education on Safe Mining of Deep Metal Mines, and School of Resources and Civil Engineering, Northeastern University, Shenyang 110819, China

² Key Laboratory of Earth and Planetary Physics, Institute of Geology and Geophysics, Chinese Academy of Sciences, Beijing 100029, China

³ Electron Microscope Laboratory, Institute of Geology and Geophysics, Chinese Academy of Sciences, Beijing 100029, China

Abstract: Amphibole is a rock-forming mineral widely existing on the earth. It is easily dissolved and altered during the later stage of diagenesis and mineralization, and often forms chloritization, which is an important indicator for prospecting. To explore amphibole's dissolution process and alteration mechanism, dissolution experiments were carried out under acidic conditions using pargasite-rich amphibole as raw material, and the effects of temperature, pH, and experiment duration on amphibole alteration were investigated. Experimental samples and products were analyzed using X-ray diffractometer, field emission scanning electron microscope, electron probe micro analyzer, and transmission electron microscopy. It was found that many pores and erosion edges are produced after amphibole dissolution, and there is a clear interface between the dissolved residual portion and the parent. The dissolved residual portion remains in the amphibole phase, but as the temperature and time increase, the intensity of the diffraction peak of the phase in the product decreases, and the peak position shifts to a small angle. Many clay minerals such as chlorite and griffithite formed on the amphibole surface. In an environment with strong acidity (pH=3), the amount of chamosite increases with temperature (180°C→210°C→240°C), whereas clinocllore is only increased in a 150–210°C environment. Griffithite growth was observed in the acidic (pH=6) and low temperature (<180°C) environments. Based on this analysis, large radius Cl⁻ enters the amphibole lattice or cracks to promote dissolution. The Al-poor and Ca- and Fe-rich regions between the edge and core of the amphibole are caused by dynamic equilibrium in amphibole dissolution and alteration process, which is an essential indicator for the beginning of amphibole dissolution-alteration. Diffusion and the coupled dissolution-precipitation mechanism accomplishes the process of dissolution and alteration to form clay minerals. The energy of the system determined by temperature and pH is the key to controlling the rate of growth and nucleation of clay minerals. High temperature and strong acidity will dissolve more iron from amphibole, which is conducive to chlorite growth. Compared to chlorite, griffithite is more sensitive to temperature. Griffithite attaches on the amphibole surface with a star-like in a weak acid and low-temperature environment. The results of this study can provide a mineralogical basis for the analysis of hydrothermal alteration processes and the division of alteration zones.

Key words: hydrothermal environment, amphibole, dissolution-alteration, chlorite, griffithite

Citation: Li et al., 2019. Experimental Study of Dissolution-Alteration of Amphibole in a Hydrothermal Environment. *Acta Geologica Sinica* (English Edition), 93(6): 1933–1946. DOI: 10.1111/1755-6724.14368

1 Introduction

Mineral alteration/phase transformation comprehensively reflects dissolution and reprecipitation in the geological environment (Putnis and John, 2010). This is an issue of geochemical processes and has an essential effect on the extensive geological processes involving geochemical element cycling (Yu and Liu, 2005; Putnis and Ruiz-Agudo, 2013; Dempster et al., 2017). In genesis analysis, metallogenic prediction, and prospecting of hydrothermal deposits, further research on mineral alteration processes and dissolution-reprecipitation coupling reactions at water

-rock reaction interfaces can yield important physicochemical information related to the source, transportation, and storage of ore deposits. This is of great significance for understanding diagenetic and metallogenic processes and distinguishing alteration marks for prospecting (Brugger et al., 2010; Zhang et al., 2015; Shen et al., 2017; Shuo et al., 2017).

Amphiboles are an essential rock-forming mineral group that can be crystallized in the crust, upper mantle, and subduction plates (Comboni et al., 2018), and records critical information on magmatic diagenesis and rock evolution (Gu et al., 2002; Baidya et al., 2016). Amphibole composition can be used as an important indicator of its classification and genesis (Gu et al., 2002;

* Corresponding author. E-mail: huangfei@mail.neu.edu.cn

Féménias et al., 2006; Xu et al., 2006), but because its crystal structure can contain almost all elements in the periodic table (Hawthorne and Oberti, 2007a), amphibole composition can become very complex due to the migration of elements and generation of secondary minerals during the alteration process.

Previous studies have demonstrated several aspects of amphibole. (1) First, amphibole is a remarkably soluble mineral, and different amphibole types have different dissolution modes, reaction rates, and ion migration modes. Inconsistent dissolution of Ca, Mg, and Si can be found in amphiboles in low-temperature (20–60°C) acidic aqueous solutions at atmospheric pressure (Schott et al., 1981). The amount of cation dissolution in titanium amphibole is mainly controlled by its crystal structure. A larger acid concentration leads to a larger leaching concentration of the cation (Shen et al., 2005). Amphibole's dissolution rate under acidic conditions is higher than under neutral and alkaline conditions at 25°C, and tremolite and anthophyllite have different dissolution rates (Rozalen et al., 2014). (2) Amphibole composition changes are systematic. HCl(aq) is one of the most important volatiles found in Earth's crust (Mei et al., 2018), and Cl content positively correlates with Fe²⁺, K, and Al contents in amphibole. The expansion of the amphibole octahedron is mainly due to Cl content development (Oberti et al., 1993). The formation of high Cl amphiboles in natural aggregates may be controlled by chemical or crystallographic factors of brine, halide, or silicate melts, and not only by Fe# in amphiboles (Campanaro and Jenkins, 2017). (3) In hydrothermal environments, amphiboles are often altered by subamphibolization, chloritization, saponification, biotitization, and epidotization. Most deposits closely related to hydrothermal processes, such as porphyry (Huang et al., 2017; Yao et al., 2018), skarn (Hong et al., 2012; Shuo et al., 2017), and hydrothermal sedimentary types, have visible alteration zoning (Liu and Fu, 2016).

Element migration and alteration of amphibole are adjustments made by geological environment changes, which are of considerable significance to the inversion of the geological environment. Calcic amphibole, of which pargasite is an important member (Féménias et al., 2006), is widely distributed in the geological setting. The physical and chemical conditions for the formation of altered products can be defined and the geochemical characteristics of ore-forming fluids can be inverted through experimental study of pargasite dissolution and related ion migration (Liu et al., 1997; Li et al., 2018). This is direct evidence for the study of ore-forming fluids and hydrothermal deposit material sources. Amphibole alteration characteristics are of great significance for determining information on the environment at the time of formation and establishing prospecting criteria.

Pargasite, which is the main mineral component of amphibole, was selected as a raw material. Systematic experiments were carried out under different temperature, pH value, and time conditions to investigate pargasite's dissolution mode and the alteration process of reprecipitation. Alteration product characteristics were observed and characterized in detail and the relationship

between amphibole's dissolution equilibrium and the nucleation growth of new clay minerals under acidic conditions was discussed. The aim of this study is to reveal the enrichment law of elements and the labelling of altered products during amphibole dissolution and reprecipitation in acidic environments. This is greatly significant to the study of geological background inversion, element migration and enrichment, and mineralization processes.

2 Experimental and Methods

2.1 Experimental instruments and processes

This experiment was completed in the Laboratory of Genesis Mineralogy, Northeastern University, Shenyang, China. The instrument used was a hydrothermal reaction system consisting of a DHG-9146A electrothermal constant-temperature blast drying chamber and a PPL hydrothermal synthesis reactor.

Amphibole was crushed into 2–4 mm particles and pure amphibole was selected for reserve. Experimental solutions with pH values of 1, 3, and 6 (recorded as S1, S3, and S6) were prepared with deionized water and reagent-grade concentrated HCl and stored in 100 ml wide-mouth bottles for reserve.

A 1g sample amphibole particles was weighed using an electronic balance and placed in the reactor and 30 ml of S1, S3, and S6 to each reactor. The reactor was then sealed and then put into a constant-temperature drying cabinet. The target temperatures (150, 180, 210, and 240°C) were set with a rate of increase of 6°C/min. When the drying chamber reached 50°C, the timing began and once the temperature reached target temperature, insulation began. After a set period (5, 10, or 20 days) the power supply was turned off and the reactor was cooled to room temperature at 1.25°C/min. The solution in the reactor was then poured into a clean beaker and the pH value of the solution after the reaction was determined. The sample was then removed and rinsed with deionized water three times to remove the reactive solution on the sample surface. The cleaned samples were then placed in the incubator with a temperature of 50°C and dried for 30 minutes to remove adsorbed water on the sample surfaces. The pressure during the experiment was generated spontaneously by the reactor without additional pressure.

2.2 Testing technology

Testing of the experimental samples and products was completed using an X'Pert Pro polycrystalline X-ray diffractometer (XRD) at the Analysis and Testing Center, Science and Technology Research Institute, Northeastern University (NEU). XRD patterns were collected between 5° and 90° (2 θ) at a scanning rate of 8.5°/min using Cu_{K α} radiation ($\lambda=0.154$ nm, 40 kV and 40 mA). Surface morphology and mineral characteristics were observed using Ultra Plus field emission scanning electron microscopy (FESEM) at the same laboratory in NEU. Chemical composition was tested using a JXA-8230 electron probe micro analyzer (EPMA) at the Guangzhou Institute of Geochemistry, Chinese Academy of Sciences. Accelerated current was 2×10^{-8} A, accelerated voltage

was 15 kV, and the spot analysis beam was 1 micron. Some energy-dispersive X-ray spectroscopy (EDS) data of the product were tested using a JXA-8530F electron probe with a 15 kV test voltage at the same laboratory in NEU. Transmission electron microscopy (TEM) analytical work was carried out using a JEOL JEM-2100 operating at a 200 kV with an electron beam generated by a LaB₆ gun at the Electron Microscopy Laboratory, Institute of Geology and Geophysics, Chinese Academy of Sciences (EML, IGGCAS).

3 Results

3.1 Original sample material

The amphibolite sample in this study was selected from Zhuji, Zhejiang Province, China. The sample's amphibole content was as high as 95 vol%, the crystal grains are coarse, and the cleavage is clear. Additionally, chlorite is formed at the edge and cleavage and the sample contains a small amount of albite (Figs. 1a, 1b). EPMA analysis showed that amphibole, chlorite, Pumpellyite, albite, and other mineral components exist in the sample. Amphibole group minerals present in the sample included pargasite, magnesiohornblende and actinolite, all of which belong to Calcic amphiboles (Fig. 1c). Table 1 shows the amphibole sample's composition. As many albite particles were

removed as possible before the experiment, thus they will not affect the investigation. The main phases in the XRD analysis were pargasite and chlorite (Fig. 3).

3.2 Post-experiment products

3.2.1 Macroscopic characteristics of solution and sample after experiment

HCl solutions with pH values of 1, 3, and 6 (S1, S2, and S3) were placed into the reactor for a blank test at 240°C for 5 days before the experiment. In this experimental group without amphibole particles, pH values did not change after 5 days, indicating that the closed state of the reactor satisfied experimental conditions requiring a closed system.

By measuring the pH of the solutions after the experiment, it was found that S1 had its pH value change to 2–3 after the experiment at 150–180°C for 5 days and 10 days and to 5–6 after the experiment at 210°C and 240°C for 20 days. Therefore, S1 underwent a significant change in pH with experimental temperature changes. After the experiment, S3 had a pH value of 5–6, making its degree of change the second largest. S6 had the smallest pH value change after the experiment. Overall, solution pH values shifted to neutral after the experiment, indicating that the solution participated in the experiment, and the pH value change was more obvious with increased

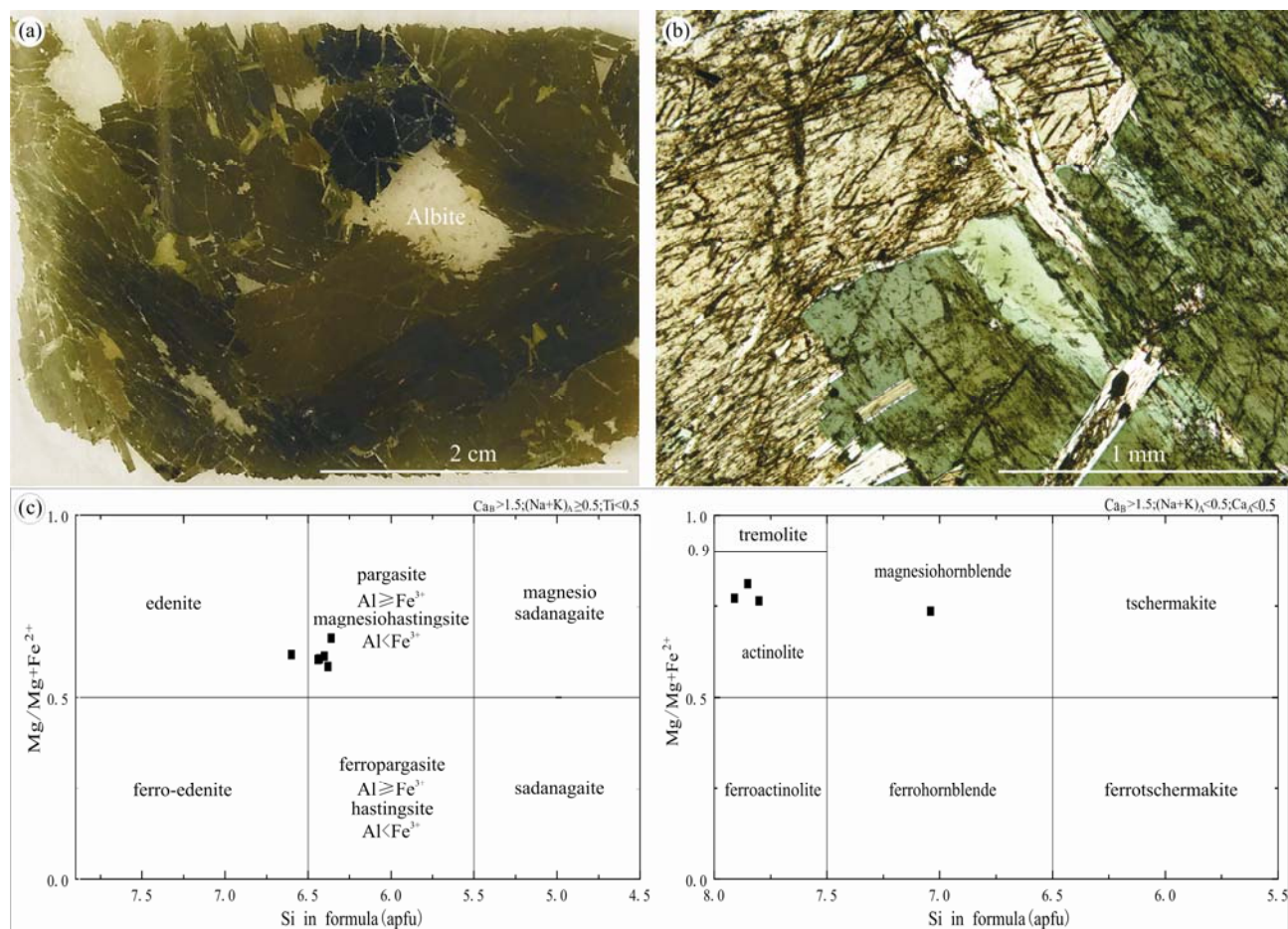


Fig. 1. Amphibole before the experiment.

(a) Microprobe slice photographs of amphibolite; (b) single polarizing microscope photographs of amphibolite; (c) classification diagrams of amphibole Mg/(Mg+Fe²⁺) vs. Si, base map from Hawthorne, F.C et al (Hawthorne and Oberti, 2007b).

Table 1 Electron microprobe analyses of amphibole (wt%)

Mineral	pargasite								actinolite					magnesiohornblende
	L-1-2	L-1-5	L-1-6	L-1-8	L-2-3	L-3-4	Average	SD	L-1-3	L-2-2	L-3-2	Average	SD	L-3-3
Oxide	43.08	43.67	43.61	44.66	43.17	43.49	43.61	0.51	55.02	56.44	56.37	55.94	0.65	49.23
SiO ₂	0.54	0.58	0.63	0.71	0.72	0.63	0.63	0.06	0.00	0.00	0.00	0.00	0.00	0.29
TiO ₂	13.12	12.88	12.82	11.02	12.76	13.10	12.62	0.73	1.35	0.97	1.00	1.11	0.17	7.54
Al ₂ O ₃	0.14	0.14	0.13	0.13	0.13	0.14	0.13	0.01	0.10	0.10	0.09	0.10	0.00	0.14
MnO	15.67	14.97	14.85	14.92	14.61	14.05	14.85	0.48	10.47	9.74	8.81	9.67	0.68	12.52
FeO	11.02	11.37	11.46	12.04	11.64	12.21	11.62	0.40	17.63	18.10	19.08	18.27	0.60	15.13
MgO	11.31	11.21	11.34	11.48	11.62	11.71	11.44	0.18	13.06	13.04	13.24	13.11	0.09	11.94
CaO	2.57	2.55	2.52	2.20	2.41	2.28	2.42	0.14	0.33	0.22	0.18	0.24	0.07	1.50
Na ₂ O	0.38	0.33	0.39	0.34	0.40	0.40	0.37	0.03	0.06	0.05	0.02	0.04	0.02	0.12
K ₂ O	0.01	0.00	0.01	0.01	0.00	0.01	0.00	0.00	0.01	0.00	0.00	0.00	0.00	0.01
Cl	97.84	97.71	97.76	97.50	97.44	98.02	97.71	0.20	98.02	98.66	98.78	98.49	0.34	98.40
Total														
Si	6.378	6.441	6.434	6.598	6.395	6.357	6.434	0.079	7.802	7.910	7.850	7.854	0.044	7.039
Al	1.622	1.559	1.566	1.402	1.605	1.643	1.566	0.079	0.198	0.090	0.150	0.146	0.044	0.961
T subtotal	8.000	8.000	8.000	8.000	8.000	8.000	8.000	0.000	8.000	8.000	8.000	8.000	0.000	8.000
Ti	0.060	0.064	0.070	0.078	0.080	0.069	0.070	0.007	—	—	—	—	0.000	0.031
Al	0.668	0.681	0.664	0.518	0.622	0.613	0.628	0.055	0.027	0.071	0.014	0.037	0.024	0.310
Fe ³⁺	0.204	0.192	0.178	0.186	0.171	0.349	0.213	0.062	0.088	0.023	0.111	0.074	0.037	0.335
Mn ²⁺	—	—	—	—	—	—	—	0.000	0.005	0.005	—	0.005	0.002	—
Fe ²⁺	1.637	1.562	1.568	1.567	1.557	1.308	1.533	0.104	1.154	1.119	0.915	1.063	0.105	1.100
Mg	2.431	2.501	2.520	2.651	2.570	2.661	2.556	0.082	3.726	3.782	3.960	3.823	0.100	3.225
C subtotal	5.000	5.000	5.000	5.000	5.000	5.000	5.000	0.000	5.000	5.000	5.000	5.000	0.000	5.001
Mn ²⁺	0.018	0.018	0.016	0.016	0.016	0.017	0.017	0.001	0.008	0.006	0.011	0.008	0.002	0.017
Fe ²⁺	0.099	0.092	0.086	0.090	0.082	0.060	0.085	0.012	0.000	0.000	0.000	0.000	0.000	0.063
Ca	1.793	1.772	1.792	1.817	1.844	1.834	1.809	0.025	1.984	1.958	1.976	1.973	0.011	1.829
Na	0.090	0.118	0.106	0.077	0.058	0.088	0.090	0.019	0.009	0.035	0.013	0.019	0.011	0.091
B subtotal	2.000	2.000	2.000	2.000	2.000	1.999	2.000	0.000	2.001	1.999	2.000	2.000	0.001	2.000
Na	0.647	0.613	0.616	0.554	0.635	0.557	0.604	0.036	0.082	0.023	0.035	0.047	0.025	0.324
K	0.073	0.062	0.073	0.065	0.075	0.075	0.071	0.005	0.010	0.009	0.004	0.008	0.003	0.022
A subtotal	0.720	0.675	0.689	0.619	0.710	0.632	0.674	0.037	0.092	0.032	0.039	0.054	0.027	0.346
OH	1.998	2.000	1.998	1.998	2.000	1.998	1.999	0.001	1.999	2.000	2.000	2.000	0.000	1.999
Cl	0.002	—	0.002	0.002	—	0.002	0.002	0.001	0.001	—	—	0.001	0.000	0.001
W subtotal	2.000	2.000	2.000	2.000	2.000	2.000	2.000	0.000	2.000	2.000	2.000	2.000	0.000	2.000
O set (non-W, fixed content)	22.000	22.000	22.000	22.000	22.000	22.000	22.000	22.000	22.000	22.000	22.000	22.000	22.000	22.000

Note: A Method for Calculating the Composition of Amphibole Electron Probe Based on Andrew J. Locock (Locock, 2014).

temperature and time (Table 2).

Amphibole particles were broken to different degrees after the experiment (Figs. 2a, 2b), and the sample in S1 showed more apparent alteration. Increased temperature yielded a greater degree of breakage. Additionally, obvious rust-colored precipitation was observed on the sample surface and reactor wall, with the appearance of rust-colored precipitates being most obvious with S3 and the presence of rust-colored precipitates increasing with temperature (Figs. 2c, 2d, 2e).

3.2.2 XRD analysis

XRD analysis indicated that the main mineral components in the samples before the experiment were pargasite and chlorite. The main mineral phases did not change after the experiment, but the peak strength and position of pargasite and chlorite changed obviously (Fig. 3).

After the experiment, the (110) and (310) diffraction peaks of pargasite changed sharply, with (240) changes followed, and slight changes to the (220) and (330) diffraction peaks. As the experimental time and temperature increased, the (110) peak gradually pinches out and the (310) peak grows relatively.

After 5 days of the experiment, the main crystal diffraction peaks of pargasite and chlorite all moved to a

Table 2 pH statistics of solutions before and after experiments

Time	Initial pH	pH value of solution after experiment			
		150°C	180°C	210°C	240°C
5 days	1	2	2	5	—
	3	6	5	6	5
	6	7	6	6	—
10 days	1	2	3	5	—
	3	6	5	6	—
	6	7	6	7	—
20 days	1	—	—	—	5

Note: "—" Represents the non-experimental group.

high angle, whereas they mostly moved to a low angle after 10 days. At the same time, the diffraction peaks of pargasite and chlorite in S6 mostly moved to a high angle, whereas they moved to a small angle with increased temperature and time for S1 and S3. Under the same solution pH and time conditions, higher temperatures yielded a more obvious shift of the diffraction peak to a small angle. These results demonstrate that longer reaction times, stronger acidity, and higher temperatures all increase crystal plane spacing, with time and temperature having the most significant effects.

3.2.3 Microscopic characteristics of samples

Secondary electron (SE) photographs of the samples

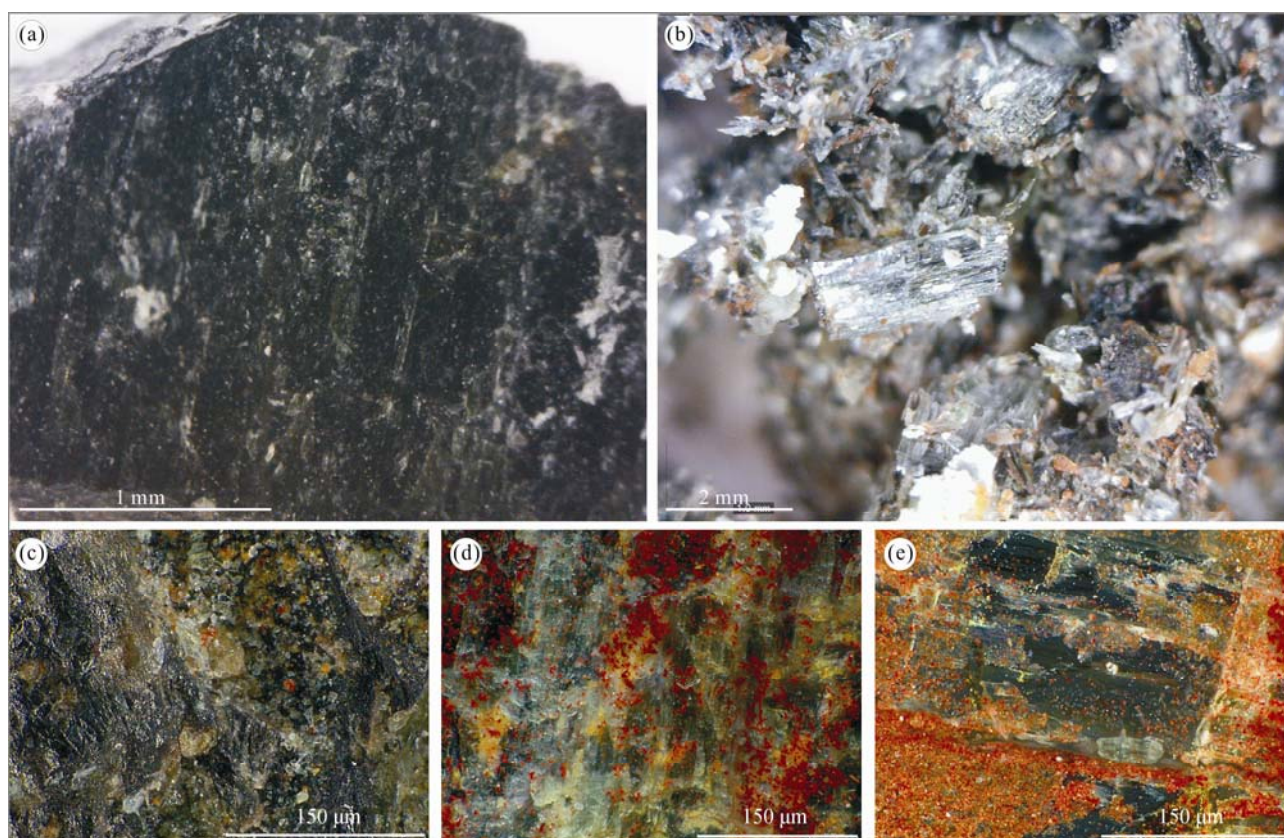


Fig. 2. Microscopic photos of samples before (a) and after (b–e) the experiment.

Amphibole in acidic solution (pH=1) was severely broken (b). After the experiment, many rust-colored precipitates (c–e) formed on the surface of samples. With increased temperature, the rust-colored precipitates increased (c. 150°C, pH=3; d. 180°C, pH=3; e. 210°C, pH=3).

showed that the amphibole surface was actively eroded in S1, with many porous and granular crystals (Fig. 4a). Some S3 samples also exhibited strong dissolution (Figs. 4b, 4c).

The dissolution of amphibole provides a material source and basement for the growth of altered minerals. To understand amphibole's dissolution process, the cross-section morphology and composition of amphibole samples after strong acid (pH=1), high temperature (240°C), and long duration (20 days) experiments were analyzed (Fig. 5). This analysis found that after the experiments, the amphibole cross-section showed obvious dissolution characteristics; however, the EPMA test indicated that it was still amphibole (Table 3). Fig. 5b shows an enlarged view of the area in Fig. 5a, with distinct zoning at the edge of the sample. From the core to the edge of the sample, Cl increased gradually (Fig. 5c), Si did not change significantly (Fig. 5d), Mg decreased significantly (Fig. 5e), Al first decreased and then increased (Fig. 5f), and Na, Fe and Ca first increased and then decreased (Figs. 5g–5i).

With changes in solution pH and temperature, chlorite and griffithite are formed after the experiment. The crystal shape is intact and particle size is uniform (Fig. 6).

Chlorite mainly grows in the environment of S3 and is lower at 150°C. Chamosite is the primary type of chlorite at 180°C, with a diameter of 1.5 microns and a small amount of clinocllore associated. With increased

temperature (180°C→210°C→240°C), the amount of cross-growth increases significantly (Figs. 6a–6d). It grows on the amphibole surface and shows a trend of diffusion. The amount of clinocllore was the greatest at 180°C and its particle size was smaller, and amounts were lower at 150°C and 210°C. A small amount of berthierine was also associated. Griffithite mainly grew in the low temperature (<180°C) environments of S6 and S3 in a star shape (Figs. 6g, 6h), with part of it growing in the form of leaves on the amphibole surface at a high angle in S3 (Fig. 6i). The amount of griffithite decreased with increased temperature.

4 Discussions

4.1 Reaction and equilibrium

Alteration is a process in which crustal rocks reach a new equilibrium under new physicochemical conditions (Li, 2018). Equilibrium is the main component of water-rock reactions. The essence of water-rock reactions is the activation, migration, and precipitation of elements between fluids and rocks under specific conditions (such as mineral stability, temperature, pressure, pH, f_{O_2} , rock porosity, stress, etc.) (Zhang et al., 2017; Zhang and Zhang, 2017). Amphibole's water-rock reaction process can be divided into three equilibrium states based on the stable state and degree of dissolution and alteration (Fig. 8).

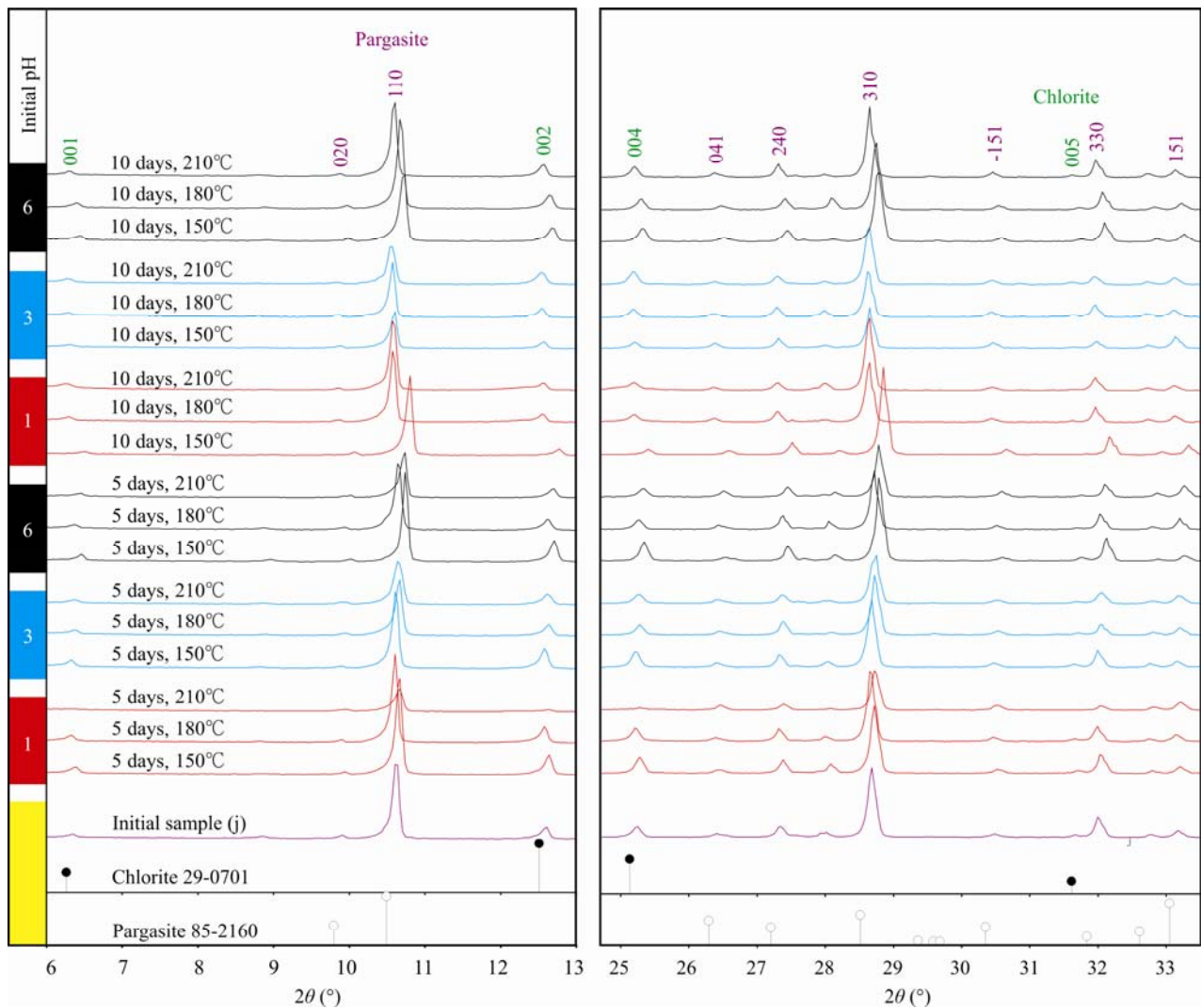


Fig. 3. XRD patterns of sample.

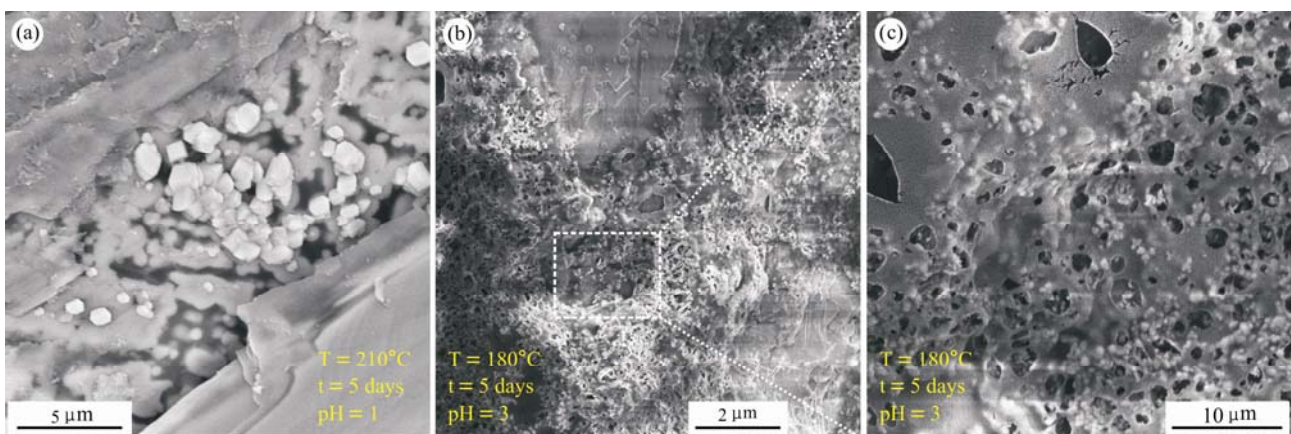


Fig. 4. SE photographs of the samples.

(a) amphibole dissolves mainly at pH = 1, and many granular substances are produced. (b, c) at initial solution pH=3, dissolution is found only on part of sample surface, and c is a local enlargement of b.

(1) First equilibrium state

Amphibole was in a stable state prior to the experiment, thus its ions in amphibole did not diffuse, migrate, or precipitate.

(2) Second equilibrium State

After the experiment, the intensity of the amphibole diffraction peak decreased obviously (Fig. 3), indicating that the amphibole had dissolved. The amount of dissolved

Table 3 Electron microprobe analyses of amphibole after experiments (wt%)

Oxide	A-4-1	A-4-2	A-4-3	A-4-4	A-4-5	A-4-6	Average	SD
SiO ₂	43.37	41.42	42.90	43.63	43.03	41.96	42.72	0.78
TiO ₂	0.63	1.03	0.56	0.60	0.68	0.49	0.66	0.17
Al ₂ O ₃	12.68	14.06	13.96	13.10	13.69	14.51	13.67	0.61
MnO	0.14	0.15	0.14	0.11	0.15	0.13	0.14	0.01
FeO	15.13	14.44	13.60	13.22	13.60	13.84	13.97	0.64
MgO	12.29	12.52	12.56	12.63	12.55	13.22	12.63	0.29
CaO	11.86	11.66	11.58	11.54	11.51	11.04	11.53	0.25
Na ₂ O	2.42	2.74	2.57	2.57	2.53	2.41	2.54	0.11
K ₂ O	0.38	0.41	0.35	0.29	0.35	0.39	0.36	0.04
Cl	0.02	0.02	0.01	0.00	0.00	0.01	0.01	0.01
Total	98.92	98.44	98.23	97.68	98.07	97.98	98.22	0.39
Si	6.31	6.05	6.24	6.39	6.27	6.07	6.22	0.13
Al	1.69	1.96	1.76	1.61	1.73	1.93	1.78	0.13
T subtotal	8.00	8.00	8.00	8.00	8.00	8.00	8.00	0.00
Ti	0.069	0.113	0.062	0.066	0.074	0.053	0.073	0.019
Al	0.480	0.464	0.634	0.653	0.620	0.542	0.566	0.075
Fe ³⁺	0.484	0.602	0.421	0.194	0.398	0.844	0.491	0.199
Fe ²⁺	1.303	1.098	1.159	1.328	1.183	0.709	1.130	0.205
Mg	2.664	2.723	2.725	2.759	2.725	2.851	2.741	0.057
C subtotal	5.000	5.000	5.001	5.000	5.000	4.999	5.000	0.001
Mn ²⁺	0.018	0.019	0.017	0.014	0.018	0.016	0.017	0.002
Fe ²⁺	0.053	0.063	0.075	0.097	0.077	0.121	0.081	0.022
Ca	1.848	1.824	1.804	1.812	1.797	1.710	1.799	0.043
Na	0.081	0.094	0.104	0.077	0.108	0.154	0.103	0.025
B subtotal	2.000	2.000	2.000	2.000	2.000	2.001	2.000	0.000
Na	0.601	0.682	0.620	0.652	0.607	0.521	0.614	0.050
K	0.071	0.076	0.066	0.054	0.065	0.071	0.067	0.007
A subtotal	0.672	0.758	0.686	0.706	0.672	0.592	0.681	0.049
OH	1.996	1.996	1.998	2.000	1.999	1.999	1.998	0.002
Cl	0.004	0.004	0.002	—	0.001	0.001	0.002	0.002
W subtotal	2.000	2.000	2.000	2.000	2.000	2.000	2.000	0.000
O set (non-W, fixed content)	22.000	22.000	22.000	22.000	22.000	22.000	22.000	22.000
Species	magnesio-hastingsite	magnesio-hastingsite	pargasite	pargasite	pargasite	magnesio-hastingsite	—	—

Note: The calculation method of amphibole EPMA composition based on Andrew J. Locock (Locock, 2014).

amphibole is the basis of clay mineral growth. To understand the dissolution degree of amphibole, the difference between the average composition of the core and edge of the amphibole and that of the original amphibole was calculated (Table 4). The changes in SiO₂, TiO₂, MnO, NaO, and K₂O content in amphibole were not obvious after the experiment, but Al₂O₃, MgO, FeO, and CaO compositions changed greatly (Fig. 7).

In the experiment, Cl⁻ is the important component that reacts with amphibole and replaces its components. Although the Cl⁻ concentration is low, its concentration is higher closer to the solution, providing strong evidence for the dissolution of amphibole (Fig. 5c). Additionally, XRD analysis shows that the diffraction peaks of pargasite and chlorite moved toward high angles after 5 days of the experiment, whereas they moved toward small angles after longer reaction times (Fig. 3). Thus, it was concluded that the amphibole and chlorite lattice will shrink over a short time due to ion diffusion, and be filled with large radius Cl⁻, increasing the spacing between the crystal planes over a long time, and thus promoting the dissolution reaction. At the same time, higher temperatures yielded a faster replacement rate. The cleavage of bonds caused by dissolution also enlarged the lattice space of amphibole and increased the possibility of Cl⁻ entering the amphibole structure.

Table 4 Amounts of core and edge components of the altered amphibole particles increased or decreased compared with the original sample

Oxide	Average	A-4-3	A-4-6	Core	Edge
SiO ₂	43.61	43.63	43.37	0.020	-0.237
TiO ₂	0.63	0.60	0.63	-0.033	0.000
Al ₂ O ₃	12.62	13.10	12.68	0.477	0.055
MnO	0.13	0.11	0.14	-0.017	0.013
FeO	14.85	13.22	15.13	-1.633	0.284
MgO	11.62	12.63	12.29	1.011	0.669
CaO	11.44	11.54	11.86	0.101	0.419
Na ₂ O	2.42	2.57	2.42	0.146	-0.001
K ₂ O	0.37	0.29	0.38	-0.080	0.012
Cl	0.00	0.00	0.02	0.000	0.016

Note: In this study, the average composition of pargasite before the experiment was taken as the composition of original amphibole, A-4-3 in the experimental posterior amphibole as the composition of the core of amphibole, and A-4-6 as the composition of the margin of amphibole.

The Si, Na, and K contents changed little before and after the experiment. This is because Si is relatively stable, so there is no reaction between Si and Cl and it is not easy to migrate to the solution (Brandt et al., 2003; Kim et al., 2017). Therefore, during amphibole dissolution, only a small amount of Si can spontaneously diffuse into the solution because of environmental changes (Figs. 5d and 7). In amphibole, Na and K mainly occupy the A position because there are vacancies in the A position (Table 1).

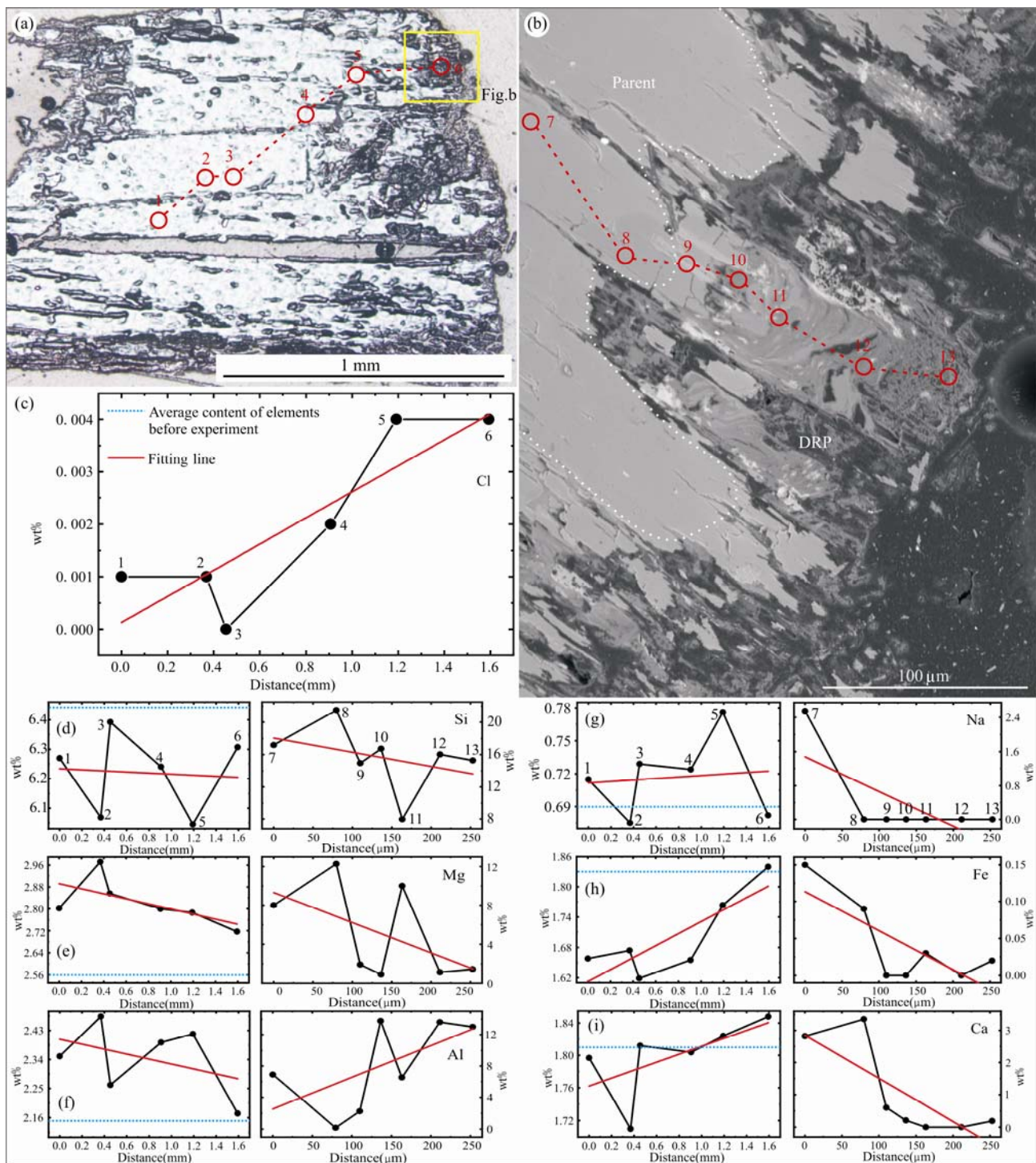


Fig. 5. Back scattered electron (BSE) photographs (a, b) and composition change maps (c–i) of sample profiles.

Red circle in figure a is the position of electron probe analyzer wavelength-dispersive X-ray spectroscopy (EPMA WDS) point analysis (1–6, Table 3), figure b is a local enlargement of figure a. The red circle in figure b is the position of EPMA EDS point analysis (7–13), and the line direction from 1 to 13 is the direction of core to edge. (c–i) The trend chart of composition change at these locations. From the core to the edge, the amphibole composition changes regularly. Cl content increases, Si and Mg content decreases, whereas Na, Fe, and Ca first increase and then decrease.

The Na and K also have space to accommodate their changes when the environment changes, so they showed no apparent characteristics of migration to the solution (Figs. 5g and 7). Moreover, chlorite and griffithite formed in this reaction have a low demand for Na, so they did not

affect the reaction.

The stable state of ion migration in amphibole will change due to the long duration of high temperature and the lengthy cooling process. The migration of Ca is mainly due to spontaneous diffusion to the solution from

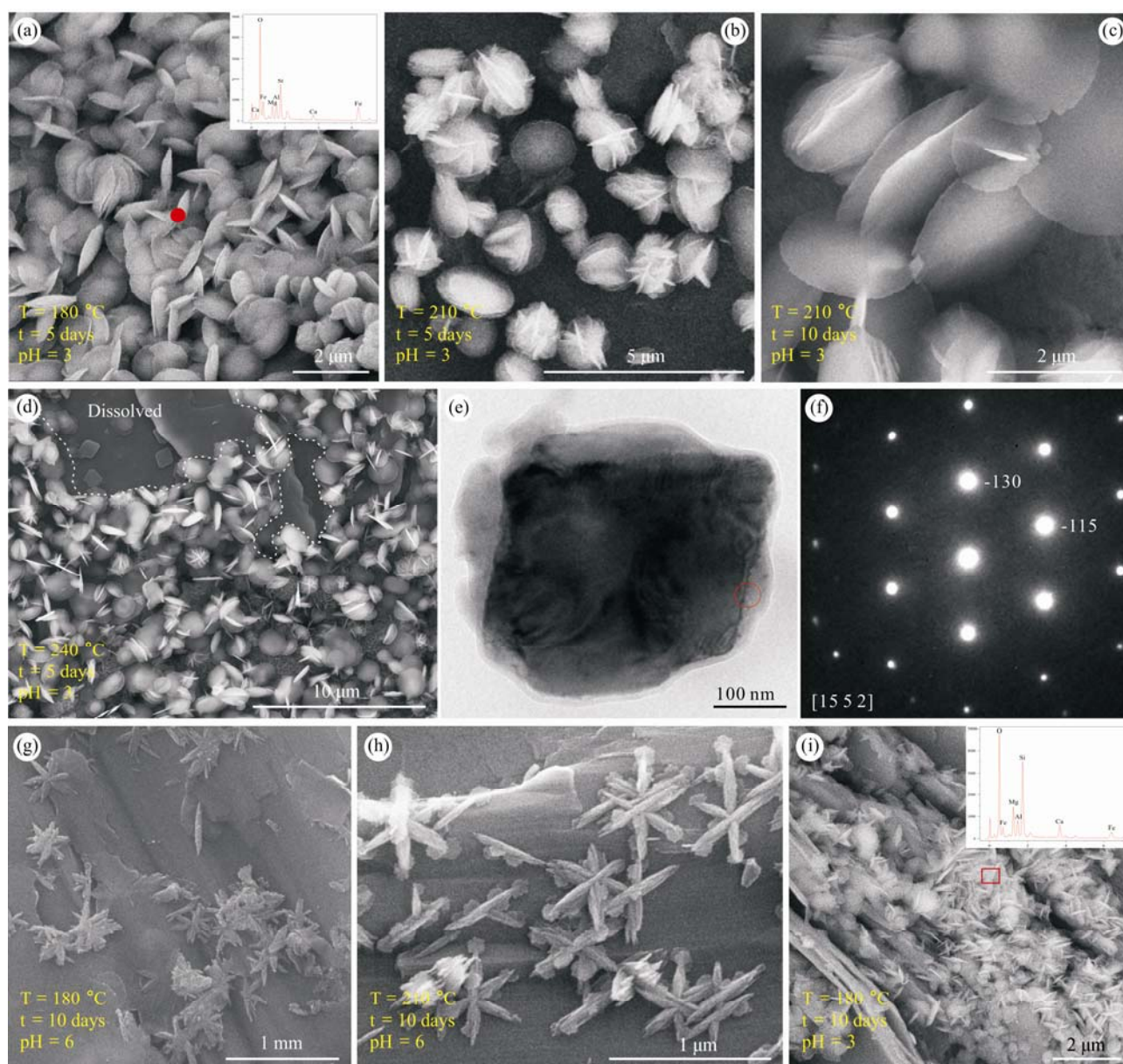


Fig. 6. SE images, EDS spectra, a bright field (BF) image, and selected area electron diffraction (SAED) patterns of clay minerals on the surface of samples after experiment.

(a–d) Chlorite grown on the surface of amphibole after experiment shows simple sheet growth at low temperature and short duration conditions. (a) Increasing temperature will increase the cross-growth and total amount of chlorite. (d) Surface materials of samples are analyzed by BF (e). (f) SAED pattern of chlorite. Griffithite mainly grows on the surface of amphibole (g, h) in the experimental environment at pH 6, whereas it grows at a high angle on the amphibole surface at pH 3 (i).

environmental changes. The system's energy decreases during the cooling process, causing the ions to move toward the amphibole. Ca has a larger radius than other cations, making it difficult to enter amphibole; therefore, a Ca enrichment zone is formed near the amphibole margin. The Fe ion has a smaller radius than Ca, thus it is easier to return to amphibole in the cooling process. However, the formation of iron-rich clay minerals on the amphibole surface consumes a lot of Fe and there were many rust-colored precipitates on the inner wall of the reactor. The content of Fe in amphibole decreased significantly after the experiment compared with the original (Figs. 5h and 7) and the decrease is more significant at the edge (Fig.

5h). There is also a Fe-rich interface between the core and the rim. As with Ca and Fe, there is a particular interface for Al content change; however, Al content increases from the interface to the edge and/or to the amphibole core (Fig. 5f). This may be due to the spontaneous migration of Al to the solution and the formation of a large amount of aluminosilicate on amphibole surface.

Amphibole dissolves continuously when in contact with the solution and pores are generated continuously. The formation of these pores enables further contact between the solution and undissolved amphibole at the interface. Connectivity between the solution and the interface makes the solution at the interface permanently unsaturated

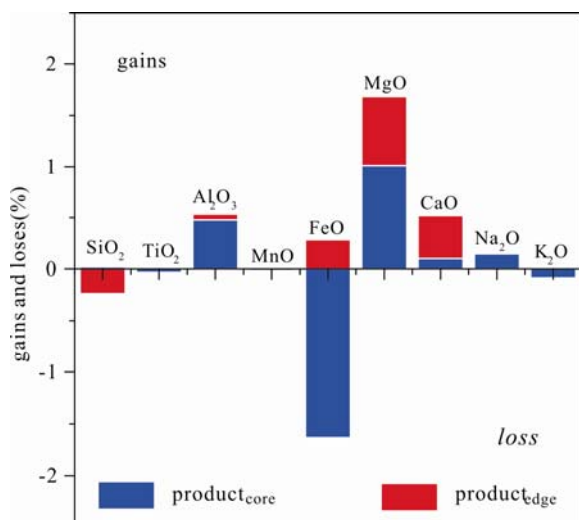


Fig. 7. The amount of the core and edge components of the altered amphibole particles increased or decreased as compared with the original sample.

relative to amphibole, causing the amphibole to continue to dissolve and continuously transport ions to the edge and solution. The composition change of the amphibole profile is obvious after dissolution.

The degree of alteration and the ion distribution state differ from the edge of the sample to the core. This indicates that the equilibrium is dynamic and moves continuously toward the center of the amphibole during dissolution. This causes the ions in amphibole to migrate through diffusion. This dissolution is weak and has not yet caused a phase transformation; therefore, the interface of

special composition change or Al-poor, Ca-rich, and Fe-rich regions may be formed by a dynamic equilibrium during amphibole dissolution, which is an essential sign of the beginning of amphibole dissolution-alteration.

(3) Third equilibrium State

There is an obvious interface between the dissolved residual part and the undissolved part (Parent) of amphibole in a hydrothermal environment (Figs. 5a, 5b). There are many dissolution holes and edges on the surface (Fig. 4) and section (Figs. 5a, 5b) of dissolved amphibole. These holes are clearly demarcated from the edge to the center and the change of corrosion along the amphibole fissures is more obvious. These structures have the characteristics of a dissolution-precipitation coupling mechanism (Putnis, 2002; Putnis, 2009; Mondal et al., 2017). The reaction begins at the edges of amphibole particles or along cracks and points to the center of amphibole. However, considering that many clay minerals are formed on the amphibole surface and the dissolved and undissolved parts of amphibole are amphibole phases, clay minerals are not formed immediately when the original amphibole dissolves.

The formation of the solid phase on parent rock surface accelerates the parent rock's dissolution and increases the formation rate (Putnis, 2002). The growth of clay minerals such as chlorite and griffithite also plays an important role in the dissolution of amphibole. Dissolution, precipitation rate, and mass transfer between altered amphibole and protoamphibole are unbalanced (Altree-Williams et al., 2015), making the reaction sustainable. Because the energy required for amphibole dissolution and clay mineral crystallization is not the same, rates of dissolution and precipitation may differ; however, there must be some

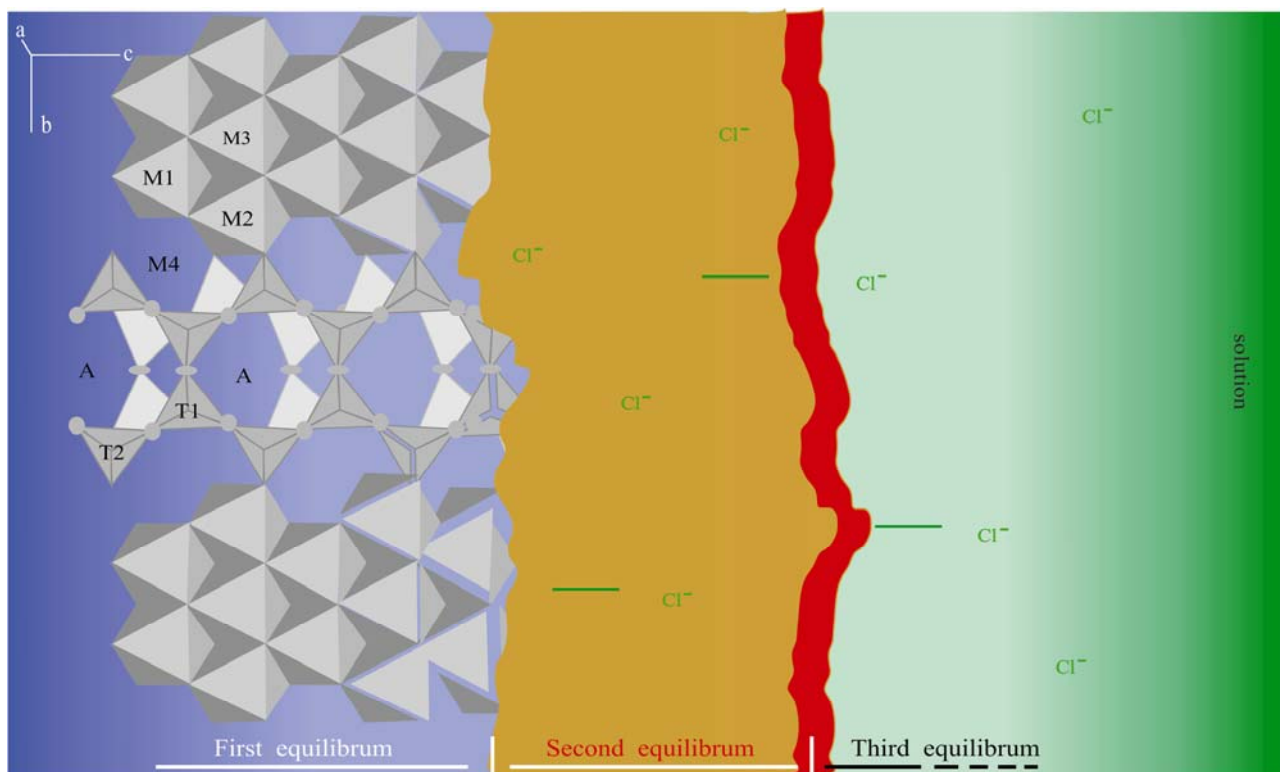


Fig. 8. Conceptual map of amphibole dissolution equilibrium and dissolution-precipitation mode.

equilibrium at the interface between amphibole and clay mineral growth. To enable clay minerals to grow, this interface can reach saturation or supersaturation, so that the amphibole phase is replaced by clay minerals such as newly formed chlorite.

The third equilibrium state is directly related to clay minerals, the growth of which begins with nucleation on the amphibole surface. For crystals, structural rearrangement occurs when the surface environment differs from that of other places, and the greater the difference, the more obvious the rearrangement (Vlieg, 2016). At the beginning of the experiment, due to the influence of temperature and pH, the composition and structure of amphibole in contact with acidic or basic solutions are constantly adjusted to achieve equilibrium. This process starts at the interface between an amphibole crystal and the solution, is related to the solution, is affected by the interface environment, and is carried out by diffusion and ion exchange. Amphibole dissolves in different degrees in the system, and the dissolved substance diffuses spontaneously into the solution, continuously increasing the concentration of the solution.

As a highly ordered crystal, amphibole can make the solution at the solid-liquid interface partially ordered, which can extend 3–5 layers. This solution is known as a quasi-liquid (Vlieg, 2016). The thin quasi-liquid skin is the crystal interface equivalent of the solvation shell found around dissolved molecules and ions in the solution (Vlieg, 2016). When the solution's ionic concentration increases to a very high value, the molecule (atom) will remove the solvation shell and penetrate into the solution-like layer of the interface, precipitate on the amphibole substrate, form small nuclei, and then grow continuously to form a clay film. However, if the system's temperature and pH make the substances dissolved in amphibole highly active in the solution and it is difficult to form crystallization sites on the base, it is difficult to form crystalline nuclei of clay minerals. At that time, the amphibole dissolution rate is higher than the clay mineral precipitation growth rate, thus in the pH=1 solution, most of the amphibole breaks up (Fig. 2b) or dissolves (Fig. 4) without clay mineral formation. At the same time, when the system conditions are not sufficient to cause amphibole to dissolve enough ions, there will be a lack necessary material source materials and fixing points for nucleation, thus there will not be a large number of clay minerals. This kind of situation is consistent with low temperature (<180°C) and weak acidity (pH=6). In systems with low energy and low supersaturation (Otálora and García-Ruiz, 2014; Atree-Williams et al., 2015), griffithite crystals can only grow on the amphibole surface at low angles to obtain sufficient material sources (Figs. 6g, 6h).

Therefore, amphibole in the first equilibrium state (stable state) enters the second equilibrium state (dynamic equilibrium) after the environmental change. Ions in amphibole migrate through diffusion because dissolution is relatively weak and amphibole has not yet undergone phase transformation; however, it provides sufficient material source for clay mineral growth in the third equilibrium state, which is the saturated state of clay

mineral growth. This state is accomplished by the dissolution of amphibole and the precipitation of chlorite, griffithite, and other clay minerals, and belongs to the coupling mechanism of dissolution and precipitation. The existence of the second equilibrium state indicates that the formation of clay minerals from amphibole, such as chlorite and griffithite, through the water-rock reaction process is the result of diffusion and dissolution-precipitation.

4.2 Relationship between Nucleation Growth Patterns of Clay Minerals and the Environment

Clay mineral formation has a wide temperature range (Cathelineau, 1988; Vidal et al., 2001; Morad et al., 2011; Beaufort et al., 2015; Wang et al., 2018). By summarizing previous studies, it was found that saponite usually grows in environments with temperatures below 100°C and in environments above 300°C (Beaufort et al., 2015). Additionally, chlorite is highly sensitive to formation environment. At present, the use of chlorite geothermometer is very common, but there are many kinds of chlorite geothermometer. Chlorite geothermometer studies have not included every kind of chlorite, which may be the main reason for the limited use range of many chlorite geothermometers. In depth study of the temperature range of different types of chlorite will bring more convenience for geological work.

Through many SE photographs of the samples after the experiment, it was found that clay mineral growth changed regularly with temperature and pH, and the regularity of chlorite and griffithite was the most obvious. Chlorite mainly consists of iron-rich chamosite and clinochlore, which grew in the environment of S3 (Figs. 6 and 9). The quantity of chamosite increases obviously with increased temperature. Oblique chlorite mainly grew in a 180°C environment and existed in a small amount in the 150°C and 210°C environments (Fig. 9). High temperature can promote amphibole dissolution and increase the iron content in environmental prospecting. Therefore, clinochlore is more sensitive to temperature than

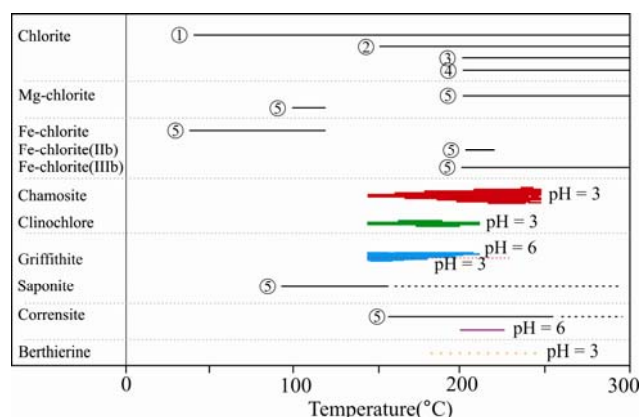


Fig. 9. The range of formation temperature and pH value of clay minerals.

the temperature range indicated by black lines in the figure is the result of predecessors: ①40–160°C (Vidal et al., 2001), ②150–300°C (Cathelineau, 1988), ③200–350°C (Morad et al., 2011), ④206–340°C (Wang et al., 2018), ⑤(Beaufort et al., 2015). The other colors are the growth temperature and pH range of clay minerals obtained in this experiment.

chamosite as chamosite needs more iron. Raising temperature is thus beneficial to the growth of chamosite.

Griffithite exists in the environment with strong acidity (pH=3) at low temperature (150°C) and weak acidity (pH=6) (Fig. 9), and it had a lower quantity than chamosite. Griffithite is a type of saponite with high iron content (Vicente et al., 1997), though its iron content is lower than that of chamosite (Griffithite Mineral Data). Compared with pargasite, clinocllore, and chamosite, the content of Al in griffithite is lower. The results show that Al dissolution in amphibole is lower at low temperature (<180°C) and weak acidity (pH=6), which are conditions not conducive to the growth of chlorite. In addition, in the pH 3 environment, griffithite is mostly leaf-like and contacts amphibole at a high angle (Fig. 6i), whereas in the pH 6 environment, griffithite is mostly attached to the amphibole surface (Figs. 6g, 6h). This may be related to the nucleation growth pattern of minerals. Griffithite is found in smaller amounts than chlorite. Therefore, high temperature, strong acidity environments and low temperature, weak acidity environments are not conducive to the formation of altered minerals.

5 Conclusions

In this study, amphibole dissolution experiments were carried out under different pH and temperature conditions and experimental cycles. After systematic observation, analysis, and discussion of the experimental results, the following conclusions are drawn:

(1) Amphibole dissolves in acidic solutions at medium and low temperatures and forms clay minerals such as chlorite and griffithite.

(2) There are three equilibrium states in the amphibole dissolution process. The first equilibrium state is the stable state of amphibole, the second equilibrium state includes the diffusion, migration, and substitution of ions between amphibole and the solution, and the third equilibrium state is the dynamic equilibrium between amphibole and new clay minerals.

(3) Al-poor and Ca- and Fe-rich regions near the quasi-liquid layer between amphibole and the solution can be used as a sign of amphibole dissolution-alteration. The formation of chlorite, griffithite, and other clay minerals by amphibole reaction results from diffusion and dissolution-reprecipitation.

(4) In pH=1 solution environment, amphiboles are mostly broken or strongly dissolved without clay mineral formation. Compared with chamosite, clinocllore is more sensitive to temperature. Chamosite needs more iron, thus raising temperature is beneficial to its growth. Griffithite can only grow on the amphibole surface at a low angle under low temperature (<180°C) and weak acidity (pH=6) conditions. High temperature, strong acidity environments, and low temperature, weak acidity environments are not conducive to the formation of clay minerals.

In this paper, the macroscopic and microscopic characteristics of samples, crystal structure characteristics, ion migration and diffusion characteristics of amphibole samples during the dissolution-alteration process, and the

growth law of clay minerals formed by alteration were systematically studied. The results obtained are helpful for a deeper understanding of the geological processes related to hydrothermal alteration and deposits related to hydrothermal alteration, such as porphyry, skarn, and hydrothermal sedimentary deposits, and provides experimental evidence. This provides empirical data for the geological environment marked by chloritization, and is of great significance for ore genesis analysis, metallogenic prediction, and prospecting practices.

Acknowledgments

This work was funded by the National Natural Science Foundation of China (41272062), Key Laboratory of Earth and Planetary Physics (IGGCAS, DQXX201706), The Fundamental Research Funds for the Central Universities (N170106001), National Nonprofit Institute Research Grant (IGGE, AS2017J13), China Postdoctoral Science Foundation (2019M651136). We sincerely thank Sun Wei, Yin Lixin, Zhang Ning, Li Huili, Wu Yan, Song Dan for their support in sample testing. We also thank Sun Yu (Guangzhou Institute of Geochemistry, Chinese Academy of Sciences) for his help in delivering and testing some samples, and Li Guanglu (Institute of Chemistry, College of Science, NEU) for his analysis of some experimental data. We also thank two anonymous reviewers and editor Liu Lian for their constructive inputs.

Manuscript received Oct. 1, 2018
 accepted Dec. 20, 2018
 associate EIC MAO Jingwen
 edited by LIU Lian

References

- Altree-Williams, A., Pring, A., Ngothai, Y., and Brugger, J., 2015. Textural and compositional complexities resulting from coupled dissolution-reprecipitation reactions in geomaterials. *Earth-Science Reviews*, 150: 628–651.
- Baidya, A.S., Paul, J., Pal, D.C., and Upadhyay, D., 2016. Mode of occurrence and geochemistry of amphibole in the Kolihan-Chandmari copper deposits, Rajasthan, India: insight into the ore-forming process. *Ore Geology Reviews*, 80: 1092–1110.
- Beaufort, D., Rigault, C., Billon, S., Billault, V., Inoue, A., Inoué, Sayako., and Patrier, P., 2015. Chlorite and chloritization processes through mixed-layer mineral series in low-temperature geological systems—a review. *Clay Minerals*, 50(4): 497–523.
- Brandt, F., Bosbach, D., Krawczyk-Barsch, E., Arnold, T., and Bernhard, G., 2003. Chlorite dissolution in the acid pH-range: A combined microscopic and macroscopic approach. *Geochimica et Cosmochimica Acta*, 67(8): 1451–1461.
- Brugger, J., McFadden, A., Lenehan, C.E., Etschmann, B., Xia, F., Zhao, J., and Pring, A., 2010. A novel route for the synthesis of mesoporous and low-thermal stability materials by coupled dissolution-reprecipitation reactions: Rimicking hydrothermal mineral formation. *Cheminform*, 64(10): 693–698.
- Campanaro, B.P., and Jenkins, D.M., 2017. An experimental study of chlorine incorporation in amphibole synthesized along the pargasite-ferro-pargasite join. *Canadian Mineralogist*, 55(3): 419–436.
- Cathelineau, M., 1988. Cation site occupancy in chlorites and illites as a function of temperature. *Clay Minerals*, 23(4): 471–485.
- Comboni, D., Lotti, P., Gatta, G.D., Merlini, M., Liermann, H.P., and Frost, D.J., 2018. Pargasite at high pressure and

- temperature. *Physics and Chemistry of Minerals*, 45(3): 259–278.
- Dempster, T.J., La Piazza, J., Taylor, A.G., Beaudoin, N., and Chung, P., 2017. Chemical and textural equilibration of garnet during amphibolite facies metamorphism: The influence of coupled dissolution-precipitation. *Journal of Metamorphic Geology*, 35(9): 1111–1130.
- Féménias, O., Mercier, J.C.C., Nkono, C., Diot, H., and Berza, T., 2006. Calcic amphibole growth and compositions in calc-alkaline magmas: Evidence from the Motru Dike Swarm (Southern Carpathians, Romania). *American Mineralogist*, 91(1): 73–81.
- Gu, L.X., Du, J.G., Zhai, J.P., Zhao, C.H., Fan, J.G., and Zhang, W.L., 2002. Eclogites of the Dabie region: Retrograde metamorphism and fluid evolution. *Acta Geologica Sinica (English Edition)*, 76(2): 166–182.
- Hawthorne, F.C., and Oberti, R., 2007a. Amphiboles: Crystal chemistry. *Reviews in Mineralogy and Geochemistry*, 67(1): 1–54.
- Hawthorne, F.C., and Oberti, R., 2007b. Classification of the amphiboles. *Reviews in Mineralogy and Geochemistry*, 67(1): 55–88.
- Hong, W., Zhang, Z.H., Jiang, Z.S., Li, F.M., and Liu, X.Z., 2012. Magnetite and garnet trace element characteristics from the Chaganuoer iron deposit in the western Tianshan mountains, Xinjiang, NW China: Constrain for ore genesis. *Acta Petrologica Sinica*, 28(7): 2089–2102. (in Chinese with English abstract).
- Huang, Y., Li, G.M., Ding, J., Dai, J., Yan, G.Q., Dong, S.L., and Huang, H.X., 2017. Origin of the newly discovered Zhunuo porphyry Cu-Mo-Au deposit in the Western part of the Gangdese porphyry copper belt in the southern Tibetan plateau, SW China. *Acta Geologica Sinica (English Edition)*, 91(1): 109–134.
- Kim, E., Ahn, H., Jo, H.Y., Ryu, J.H., and Koh, Y.K., 2017. Chlorite alteration in aqueous solutions and uranium removal by altered chlorite. *J Hazard Mater*, 327: 161–170.
- Li, K., Brugger, J., and Pring, A., 2018. Exsolution of chalcopyrite from bornite-digenite solid solution: an example of a fluid-driven back-replacement reaction. *Mineralium Deposita*, 53(7): 903–908.
- Li, M., 2018. Study on the hyperspectral characteristics and hydrothermal alteration of the drill core from ChuDuogu Lead-Zinc deposit in Tuotuo river area, Qinghai Province. (M.S.Thesis), China: China University of Geosciences (Beijing), 1–66.
- Liu, S.F., and Fu, S.X., 2016. A research review of iron oxide Copper-Gold deposits. *Acta Geologica Sinica (English Edition)*, 90(4): 1341–1352.
- Liu, Z.H., Yuan, D.X., and He, S.Y., 1997. Stable carbon isotope geochemical and hydrochemical features in the system of carbonate-H₂O-CO₂ and their implications evidence from several typical Karst Areas of China. *Acta Geologica Sinica (English Edition)*, 71(4): 446–454.
- Locock, Andrew J., 2014. An Excel spreadsheet to classify chemical analyses of amphiboles following the IMA 2012 recommendations. *Computers and Geosciences*, 62: 1–11.
- Mei, Y., Liu, W., Brugger, J., Sherman, D.M., and Gale, J.D., 2018. The dissociation mechanism and thermodynamic properties of HCl(aq) in hydrothermal fluids (to 700°C, 60 kbar) by ab initio molecular dynamics simulations. *Geochimica et Cosmochimica Acta*, 226: 84–106.
- Mondal, S., Upadhyay, D., and Banerjee, A., 2017. The origin of rapakivi feldspar by a fluid-induced coupled dissolution-precipitation process. *Journal of Petrology*, 58(7): 1393–1418.
- Morad, S., Sirat, M., El-Ghali, M.A.K., and Mansurbeg, H., 2011. Chloritization in proterozoic granite from the Aspö laboratory, southeastern Sweden: record of hydrothermal alterations and implications for nuclear waste storage. *Clay Minerals*, 46(3): 495–513.
- Oberti, R., Ungaretti, L., Cannillo, E., and Hawthorne, F.C., 1993. The mechanism of Cl incorporation in amphibole. *American Mineralogist*, 78(7): 746–752.
- Otálora, F., and García-Ruiz, J., 2014. Nucleation and growth of the Naica giant gypsum crystals. *Chemical Society Reviews*, 43(7): 2013–2026.
- Putnis, A., 2002. Mineral replacement reactions: from macroscopic observations to microscopic mechanisms. *Mineralogical Magazine*, 66(5): 689–708.
- Putnis, A., 2009. Mineral replacement reactions. *Reviews in Mineralogy and Geochemistry*, 70(1): 87–124.
- Putnis, A., and John, T., 2010. Replacement processes in the earth's crust. *elements*, 6(3): 159–164.
- Putnis, C. V., and Ruiz-Agudo, E., 2013. The mineral-water interface: where minerals react with the environment. *Elements*, 9(3): 177–182.
- Rozalen, M., Ramos, M.E., Gervilla, F., Kerestedjian, T., Fiore, S., and Huertas, F.J., 2014. Dissolution study of tremolite and anthophyllite: pH effect on the reaction kinetics. *Applied Geochemistry*, 49: 46–56.
- Schott, Jacques., Berner, Robert A., and Sjöberg, E Lennart., 1981. Mechanism of pyroxene and amphibole weathering—I. Experimental studies of iron-free minerals. *Geochimica et Cosmochimica Acta*, 45(11): 2123–2135.
- Shen, A.J., Hu, A.P., Pan, L.Y., and She, M., 2017. Origin and distribution of grain dolostone reservoirs in the cambrian Longwangmiao formation, Sichuan Basin, China. *Acta Geologica Sinica (English Edition)*, 91(1): 204–218.
- Shen, H.T., Xue, J.Y., and Cai, Y.F., 2005. Dissolution mechanisms of kaersutite under different hydrochloric acid concentrations. *Acta Mineralogica Sinica*, 25(4): 347–352. (in Chinese with English abstract).
- Shuo, Y., Changqian, M., and Robinson, P.T., 2017. Textures and high field strength elements in hydrothermal magnetite from a skarn system: implications for coupled dissolution-precipitation reactions. *American Mineralogist*, 102(5): 1045–1056.
- Vicente, M.A., Soares, M., Baneres-munoz, M.A., and Martinpozas, J., 1997. Characterization of the solids obtained by pillaring of griffithite (high iron content saponite) with Al-Oligomers. *Clays and Clay Minerals*, 45(5): 761–768.
- Vidal, O., Parra, T., and Trotet, F., 2001. A thermodynamic model for Fe-Mg aluminous chlorite using data from phase equilibrium experiments and natural pelitic assemblages in the 100°C to 600°C, 1 to 25 kb range. *American Journal of Science*, 301(6): 557–592.
- Vlieg, E., 2016. The role of surface and interface structure in crystal growth. *Progress in Crystal Growth and Characterization of Materials*, 62(2): 203–211.
- Wang, Z.Q., Chen, B., Yan, G.Q., and Li, S.W., 2018. Characteristics of hydrothermal chlorite from the Niujuan Ag-Au-Pb-Zn deposit in the north margin of NCC and implications for exploration tools for ore deposits. *Ore Geology Reviews*, 101: 398–412.
- Xu, D.R., Xia, B., Bakun-Czubarow, N., Ma, C., Li, P.C., Bachlinsk, R., and Chen, G.H., 2006. Metamorphic characteristics of the chenxing metabasite massif in Tunchang area, Hainan island, South china and its tectonic implication. *Acta Petrologica Sinica*, 22(12): 2987–3006. (in Chinese with English abstract).
- Yao, X.F., Liu, J.J., Tang, J.X., Zheng, W.B., and Zhang, Z., 2018. Fluid evolution and ore-forming processes of the Jiama Cu deposit, Tibet: Evidence from fluid inclusions *Acta Geologica Sinica (English Edition)*, 92(1): 127–143.
- Yu, W.H., and Liu, C.Q., 2005. Sorption of Zr⁴⁺ and Hf⁴⁺ onto hydrous ferric oxide and their fractionation behaviors: An experimental study. *Acta Geologica Sinica (English Edition)*, 79(3): 343–348.
- Zhang, B.L., Shan, W., Li, D.P., Xiao, B.J., Wang, Z.L., and Zhang, R.Z., 2017. Hydrothermal alteration in the Dayingezhuang gold deposit, Jiadong, China. *Acta Petrologica Sinica*, 33(7): 2256–2272. (in Chinese with English abstract).
- Zhang, S.Y., and Zhang, H.F., 2017. Element mobility and fluid characteristics during pyrophyllite alteration: A case study from the Baiyun pyrophyllite deposit, Wutai county, Shanxi Province. *Acta Petrologica Sinica*, 33(6): 1872–1892. (in Chinese with English abstract).
- Zhang, Z.C., Li, N., Ji, X.Z., Han, Z., Guo, Y.Y., and Li, Z.C.,

2015. Hydrothermal alteration of the Anba deposit, Yangshan gold belt, western Qinling. *Acta Petrologica Sinica*, 33(11): 3405–3419. (in Chinese with English abstract).

About the corresponding author



HUANG Fei is a Ph.D., Professor, and Ph.D. supervisor engaged in genetic mineralogy. In 2001, she founded the Laboratory of Genetic Mineralogy, Northeastern University. She led a research group to carry out genetic mineralogy research on deposits related to magmatism, metamorphism, hydrothermal, and sedimentation. She has developed a systematic experimental method for the study of genetic mineralogy. E-mail:

huangfei@mail.neu.edu.cn.

About the first author



LI Yongli has studied in the Northeastern University since 2012, received a bachelor's degree in Resource Exploration Engineering in 2016 and a master's degree in Mineral Prospecting and Exploration in 2018. Now, she is pursuing her Ph.D. in Geological Resources and Geological Engineering. Her research focuses on genetic mineralogy and experimental mineralogy. Her supervisor is Professor Huang Fei. E-mail: liyongli@stumail.neu.edu.cn.